

## Chapter 4

### Compact field-portable off-axis self-referencing DHIM

Chapter 3 dealt with the construction and application of two-beam DHIM based on Mach-Zehnder interferometer geometry. Quantitative phase output of the microscope was used to extract blood cell parameters, which were used to discriminate and identify them. In MZ-DHIM (Fig. 3.11), the object and the reference beams travel along different paths and are steered by different optical elements. This will result in the beams picking up un-correlated path length variation (due to change in mirror positions, change in optical path of air along the beams etc) unwanted temporal phase fluctuations, leading to lower temporal stability. The measured temporal stability of two-beam MZ-DHIM was 1.8nm over a period of 120s, with vibration isolation. Thickness fluctuations of red blood cells are of the order of few nanometers to few tens of nanometers [78]. To measure such fluctuations, sub-nanometer level temporal resolution is necessary, which the MZ-DHIM cannot provide. The use of optical elements for beam splitting, beam steering and beam combining leads to bulky setups, which are not field portable. Common path setup in which the object and the reference beams travel along the same path encountering the same set of optical elements will lead to appreciable improvement in temporal stability [77-99]. Common path setup manipulates the object beam to create a reference. It can be implemented either by supplanting the object beam and converting one of them into a separate reference beam [77-89] or using a portion of the object beam un-modulated by object information as the reference [90-99]. The technique which uses un-modulated portion of the object wavefront is called as the self-referencing method. Self-referencing DHIM techniques that can be implemented using only few optical components [90-99].

#### 4.1 Self-referencing DHIM – Concept

As the name suggests self-referencing DHIM generates reference wave from a portion of the object wavefront. Fig. 4.1 shows the basic concept of a self-referencing DHIM. The laser beam illuminating the object is passed through the magnifying lens. The beam after the magnifying lens is duplicated using a beam duplicator and are superposed to generate the interference patterns or holograms. Instead of using a beam duplicator, a portion of the beam can be folded back on to itself to create holograms. The beam duplicator can be a beamsplitter, a glass plate, a bi-prism, a mirror or a diffraction grating [90-99].

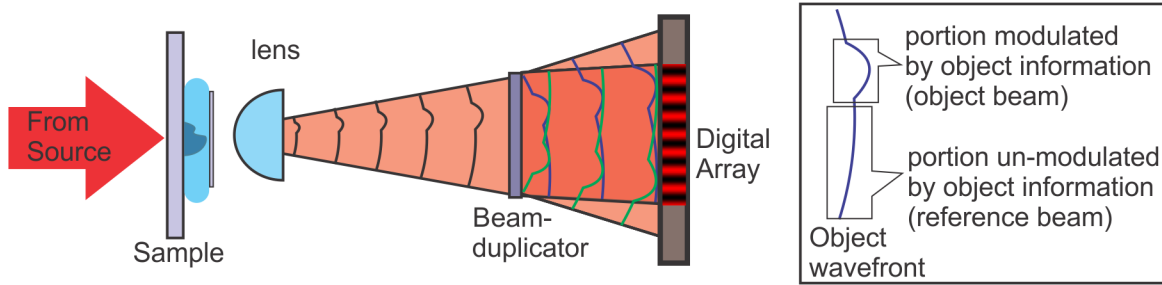


Fig. 4.1: Basic concept of self-referencing DHIM [17, 106]

The beam duplicator introduces an angle between the two versions of the object wavefront so that they interfere at an angle at the sensor plane creating an off-axis geometry (Fig. 4.1). Since in the case of self-referencing system, the interference occurs between portions of the wavefront which is modulated by object information and portion of the same object wavefront, which is un-modulated by object information, the resulting interference patterns can be treated and holograms and reconstructed numerically using the same techniques described in Section 3.1 and 3.2. Self-referencing DHIM can be implemented using amplitude division and wavefront division interferometry. But one of the easiest method is to use a glass plate to create two laterally sheared versions of the object wavefront and make then interfere to create holograms.

#### 4.2 Lateral shearing self-referencing DHIM – Concept

Lateral shearing interference geometry is one which requires very few optical elements and very easy to implement. The advantage of the geometry is that very compact 3D microscopes can be designed and fabricated. Fig. 4.2 shows the basic structure of lateral shearing digital holographic interference microscope (LS-DHIM) [17, 93]. Beam from a laser source illuminates the sample, which is magnified by a lens of appropriate magnification and numerical aperture. The beam from the lens is then split into laterally sheared versions by a glass plate. These two laterally sheared versions are made to superpose at the digital array resulting in interference patterns. Inset of the figure shows the wavefronts reflected from the front and back surface of the glass plate, superposing at the sensor plane.

There are two possibilities with a laterally sheared wavefronts superposing. In the first scenario, the amount of shearing between the two wavefronts is smaller than the size of the magnified object as shown in Fig. 4.3b [17]. In this scenario, the images from the front and back surface of the glass

plates overlap, leading to creation of shearing fringes, which in the case of an RBC can be seen in Fig. 4.3d. Such type of fringe pattern contains the gradient phase information [95, 133].

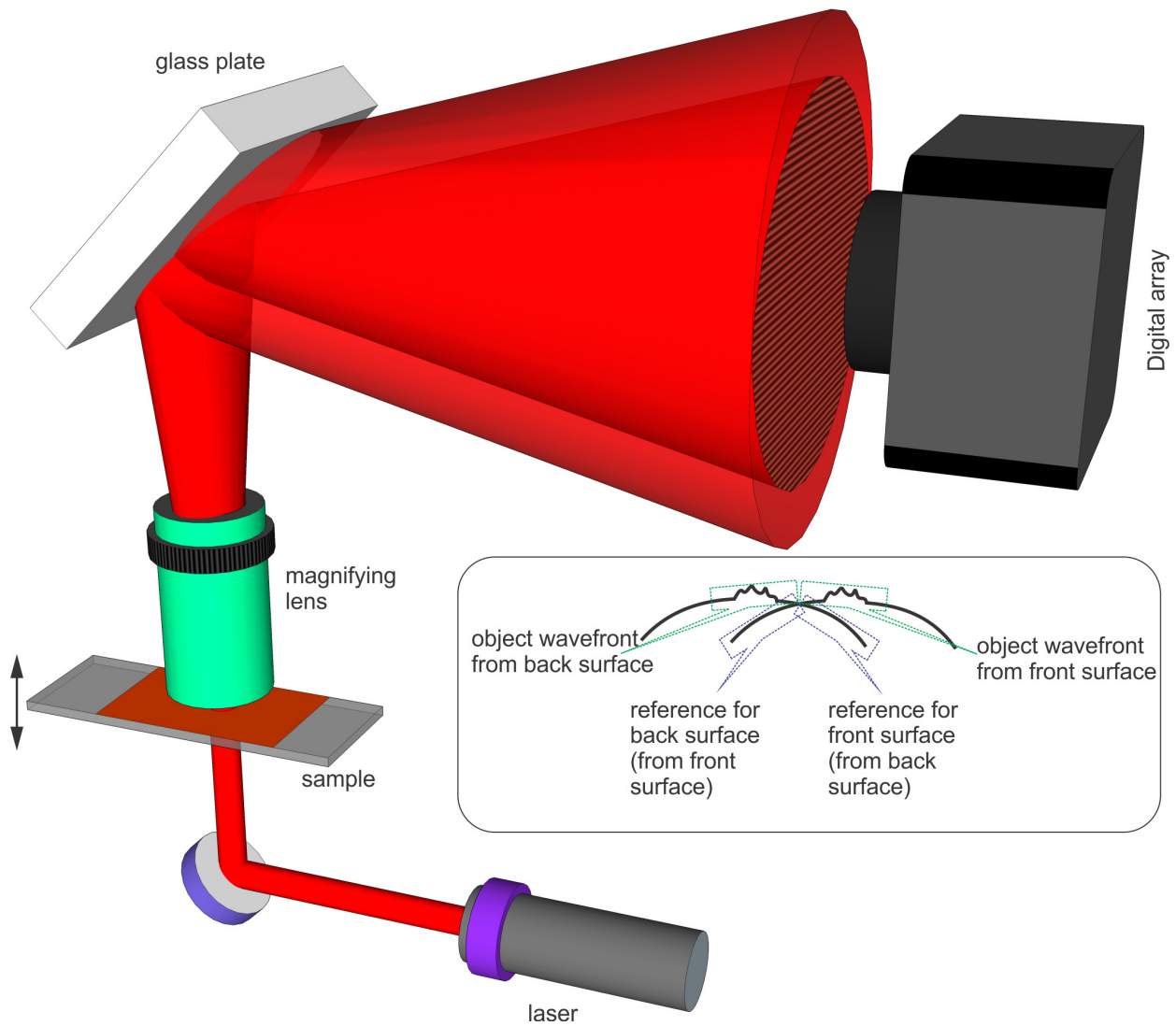


Fig. 4.2: Basic concept of Lateral Shearing DHIM [17, 93]

The second scenario shown in Fig. 4.3b [17], depicts the case in which the shear is larger than the size of the magnified object (images). In this case the portion of the wavefront reflected from the back surface, un-modulated by object information acts as the reference for the portion of the wavefront containing object information reflected from the front surface and vice versa. This can be seen from the inset of Fig. 4.2 also. It can also be noted that the direction of the wedges formed by the object wavefronts from front and back surfaces made with the reference wavefronts from

back and front surfaces are opposite, leading to fringes curved in opposite directions. These fringe systems represent off-axis holograms, since they are formed by the object and a separate reference wavefront interfering at an angle. Hologram of RBC formed due to a shearing plate is shown in Fig. 4.3e.

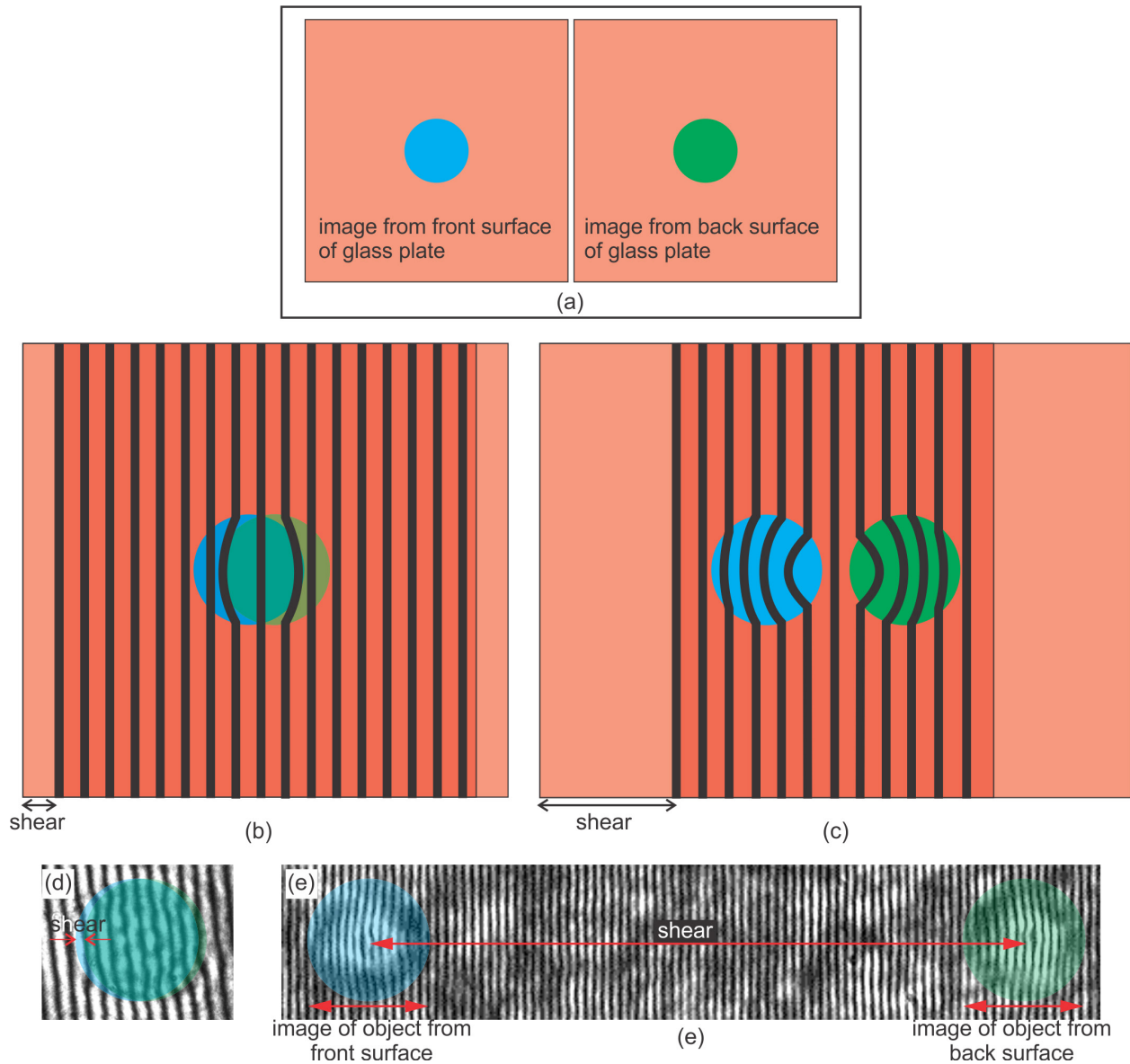


Fig. 4.3: Superposition of wavefronts reflected from the front and back surface of a glass plate show in Fig. 4.3a. (b) Scenario in which the amount of shearing less than the size of the magnified image of the object leading to formation of shearogram [90]. (c) Scenario in which the shearing is larger than the size of the magnified image of the object leading to hologram formation. (d) Shearogram and (e) Hologram in the case of RBC.

Interference patterns shown in Fig. 4.3e can be numerically reconstructed using the procedure for hologram mentioned in the previous chapter. This numerical processing yields the phase distribution of the entire object, unlike in the case of shearograms, where only the gradient phase information is available.

### 4.3 Lateral shearing self-referencing DHIM – Laboratory unit (using CCD array)

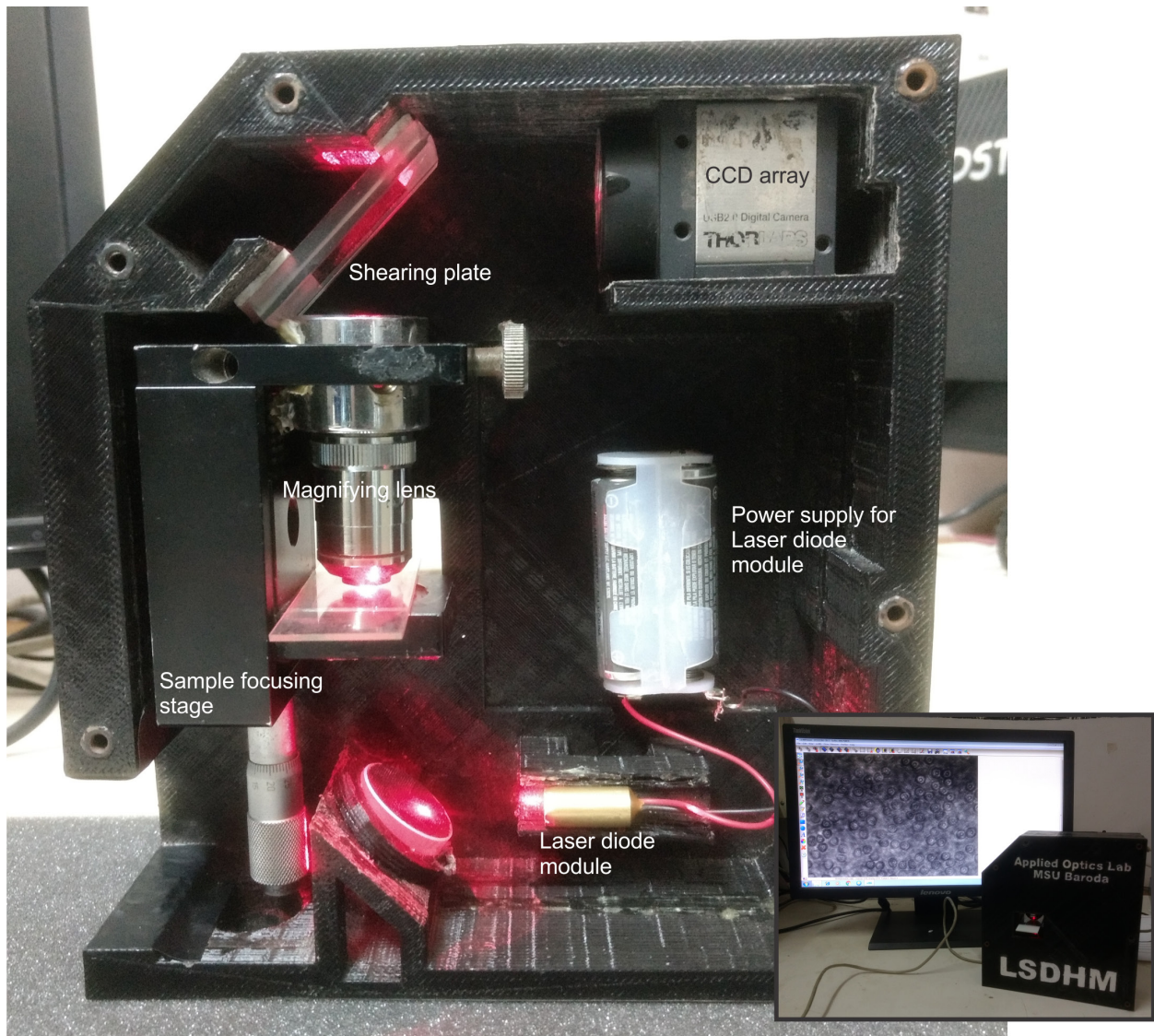


Fig. 4.4: Lateral Shearing DHIM (prototype version 1.0). It uses a laser diode module as the source and a 5mm thick fused silica glass plate for shearing. The one shown above uses a 40 $\times$ , NA=0.65 microscope objective for object magnification. Inset shows the device attached to a PC for live cell imaging.

Fig. 4.4 shows the prototype of the LS-DHIM. It uses a laser diode module (635nm, output power less than 2mW) to illuminate the object. A laser beam can also be coupled to the device from

outside to illuminate the object. So, He-Ne lasers source (632.8nm, output power 0.8mW) was also used in 3D imaging of the cells. A 40×, NA=0.65 microscope objective was used for object magnification. To achieve higher field of view, a 20×, NA=0.4 microscope objective was also used. An 8-bit, 4.65μm pixel pitch CCD array was used to record the holograms.

Setup was calibrated by recording holograms of 10μm±1μm diameter polystyrene microspheres (polysciences) of refractive index 1.52 immersed in microscope oil (refractive index 1.56). Section of the recorded hologram is shown in Fig. 4.5a. Reference hologram with the region containing the immersion oil in the field of view was recorded for phase subtraction (Fig. 4.5b). These holograms were recorded using a 20×, NA=0.4 microscope objective.

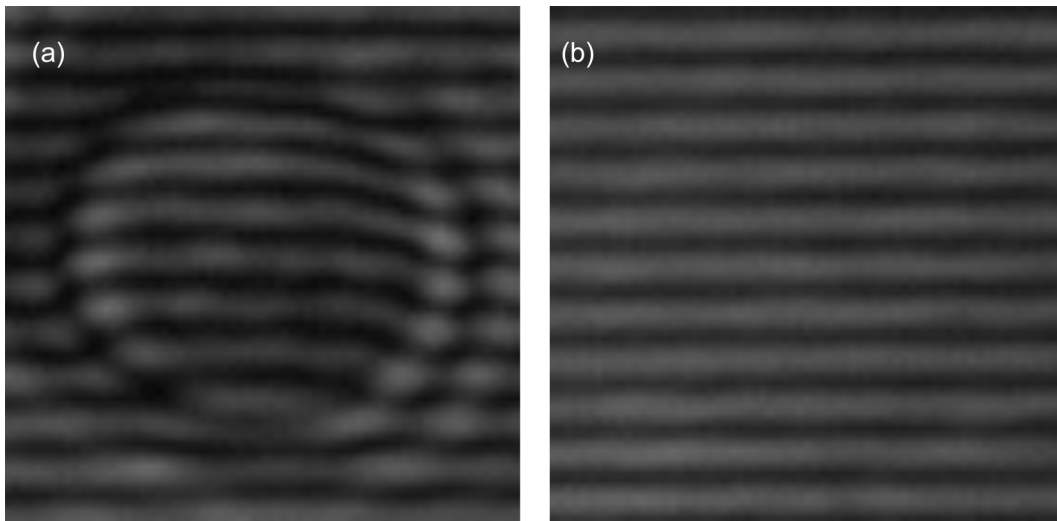


Fig. 4.5: (a) Hologram of 10μm diameter polystyrene microsphere. (b) Reference hologram used for phase subtraction.

Holograms shown in Fig. 4.5 are numerically processed as discussed in Chapter 3 and their phases extracted. The subtraction of reference phase from the object phase yields the quantitative phase image of the object shown in Fig. 4.6a. This phase distribution along with the refractive index values of the polystyrene microsphere and the immersion oil provides the thickness profile of the object shown in Fig. 4.6b. The 3D imaging capability of the device can be seen from the measured cross-sectional thickness profile of the microsphere shown in Fig. 4.6c. It can be seen from this figure that the measured thickness is close to the manufacturer specified value. The diameter measurement was repeated on several microspheres and the mean of the measured diameter was  $9.67\pm 0.82\mu\text{m}$ .

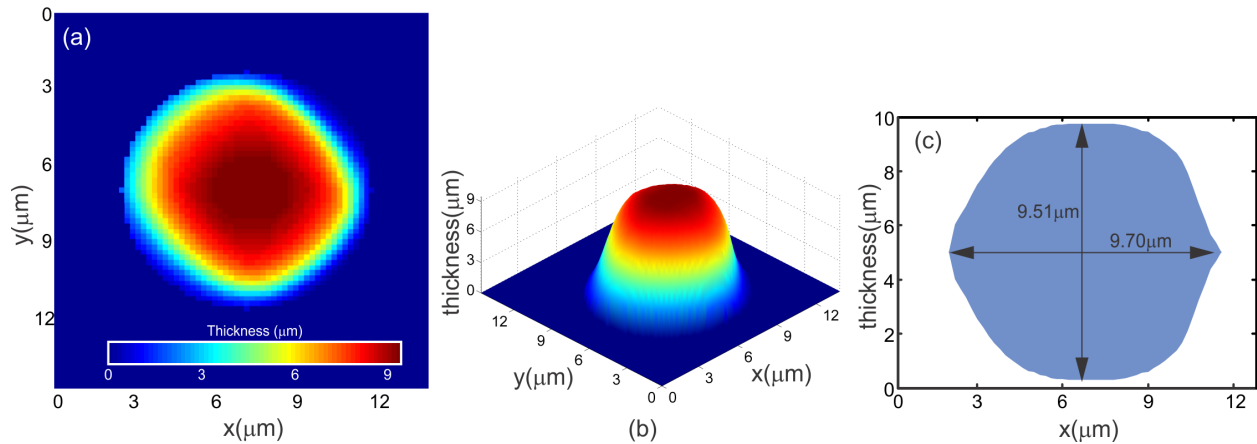


Fig. 4.6: (a) Phase contrast image of polystyrene microsphere. (b) Three-dimensional rendering of the thickness profile of the microsphere. (c) Cross-sectional thickness profile.

The minimum measurable thickness depends upon the amount of unwanted phase variation present in the system without the object present in the system (Fig. 4.7a). Standard deviation of this phase variation (Fig. 4.7b) serves as the axial resolution of the system.

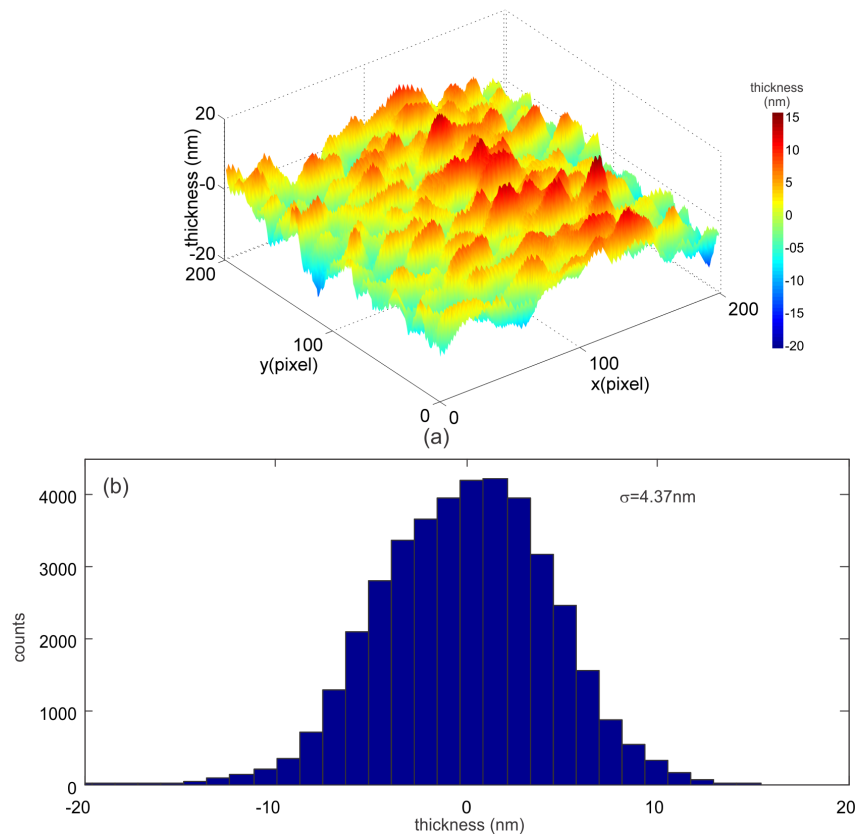


Fig. 4.7: (a) Spatial variation in thickness obtained without any object in the field of view. The standard deviation of the thickness variation acts as the quantifier for spatial stability. (b) Histogram of the thickness variation along with the standard deviation of the distribution.

The device was then used for quantitative phase imaging of red blood cells. Fig. 4.8a shows the recorded hologram of red blood cells using the device shown in Fig. 4.4. Modulation of interference fringes due to blood cells is clearly visible in Fig. 4.8b. Holograms were then numerically processed as described in Sections 3.1 and 3.2 (Chapter 3) and the thickness profiles of red blood cells were computed, which is shown in Fig. 4.8c.

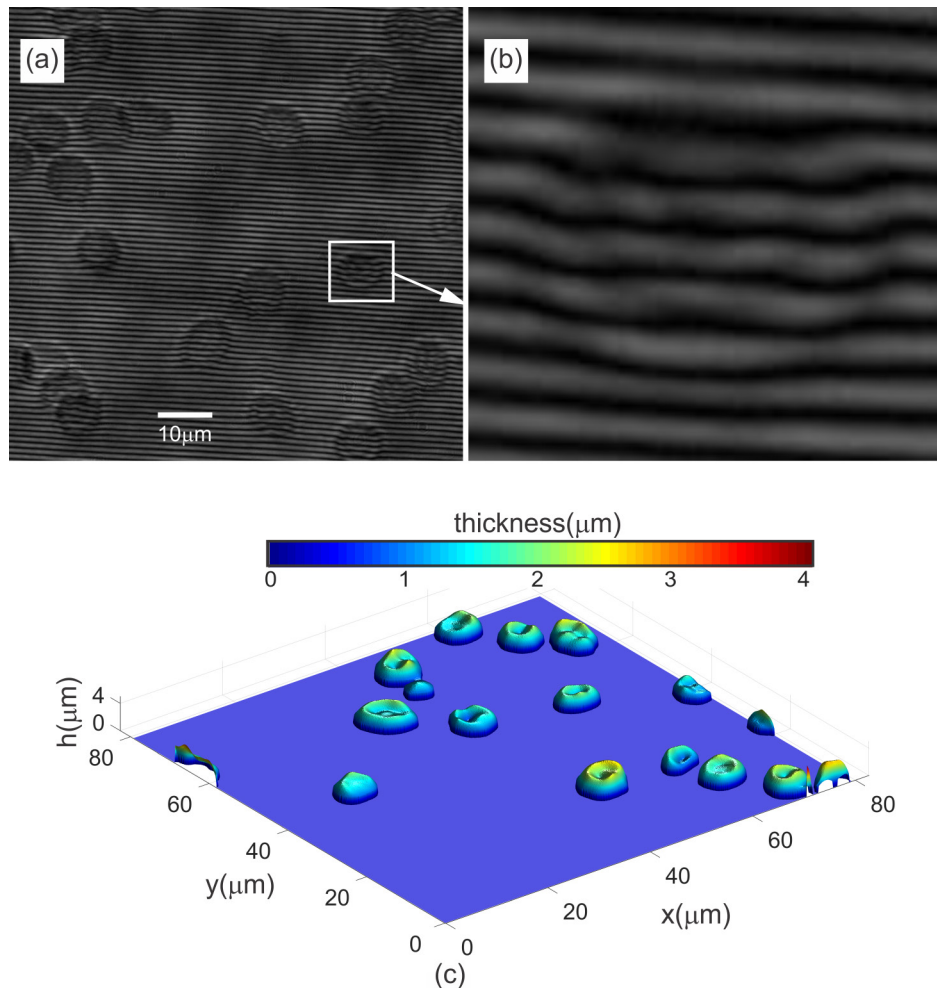


Fig. 4.8: (a) Hologram of red blood cells recorded with device shown in Fig. 4.4. (b) Region of interest inside the white box. (c) Computed thickness distribution from the reconstructed phase.

Measurement of thickness fluctuations of cells, especially red blood cells require high temporal stability. An advantage of the lateral shearing setup other than its compact nature is its high temporal stability due to its common path nature. The temporal stability of the device was measured by recording a series of holograms of a blank slide at the rate of 30Hz for 30s (total of 900 holograms) and then computing the average of the thickness fluctuation (standard deviation of thickness change along the time axis) for 10000 random space points in the field of view. The

histogram of the spatially varying thickness fluctuation is shown in Fig. 4.9. The mean of these values act as the quantifier of temporal stability.

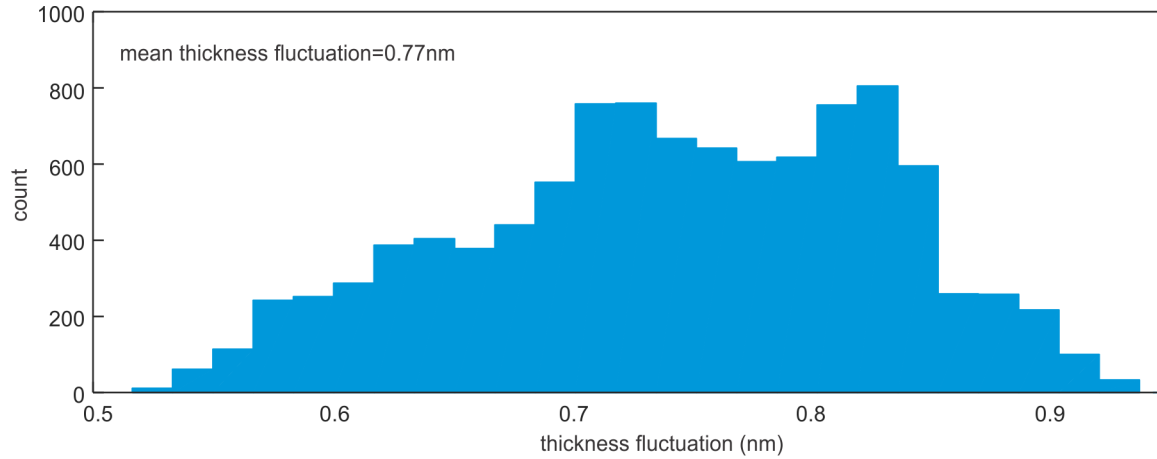


Fig. 4.9: Temporal stability of the device shown in Fig. 4.4

The device was then used to measure the cell thickness fluctuations. Towards this 300 holograms of thin blood smear (at the rate of 30Hz) were recorded and reconstructed. The standard deviation of time varying thickness at each point provides the thickness fluctuation of the cells as shown in Fig. 4.10a. Time varying thickness fluctuation was computed by sectioning the thickness variation into 1s bins (Fig. 4.10b).

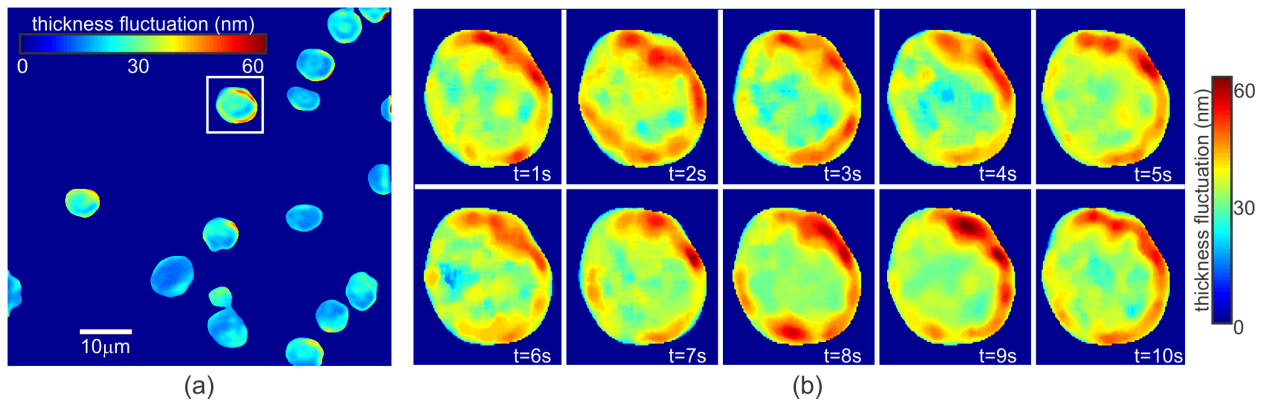


Fig. 4.10: Thickness fluctuation measurement of red blood cells. (a) Thickness variation across the field of view (computed from 300 holograms). (b) Time varying thickness fluctuation for the cell inside the white box (computed from 30 holograms which represents 1s)

#### 4.4 Lateral shearing self-referencing DHIM – Portable unit (using webcam array)

Point-of-care applications require quantitative phase microscopes which are much more compact than the device shown in Fig. 4.4. Also for wide deployment, cost of the device also need to be kept to a minimum and the devices should be easy to operate. Keeping all of these point in mind, a portable version of the LS-DHIM was designed using lens from DVD optical pick-up units for

magnification and webcam array for recording of the holograms. Fig. 4.11 shows the schematic of the portable device. The alignment of optical components and the path of the laser beam inside the device is shown in Fig. 4.11a. The stand-alone packaged device is shown in Fig. 4.11b. Photograph of the device is shown in Fig. 4.12.

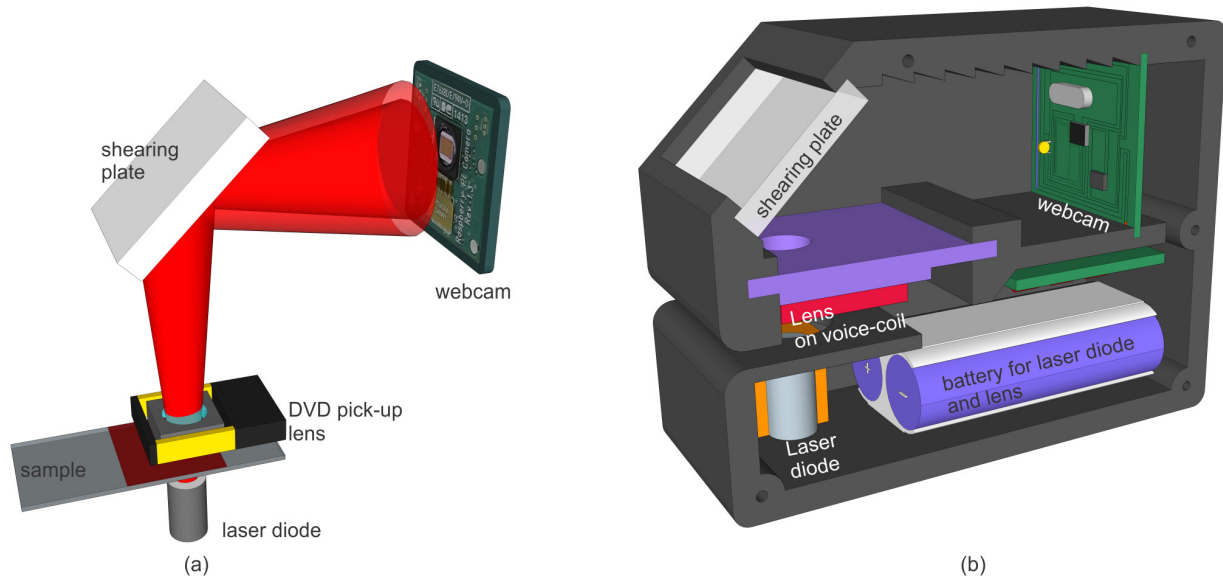


Fig. 4.11: Schematic of the field portable version of LS-DHIM. (a) Alignment of optical components and the light path in the device. (b) Inside view of the packaged device.

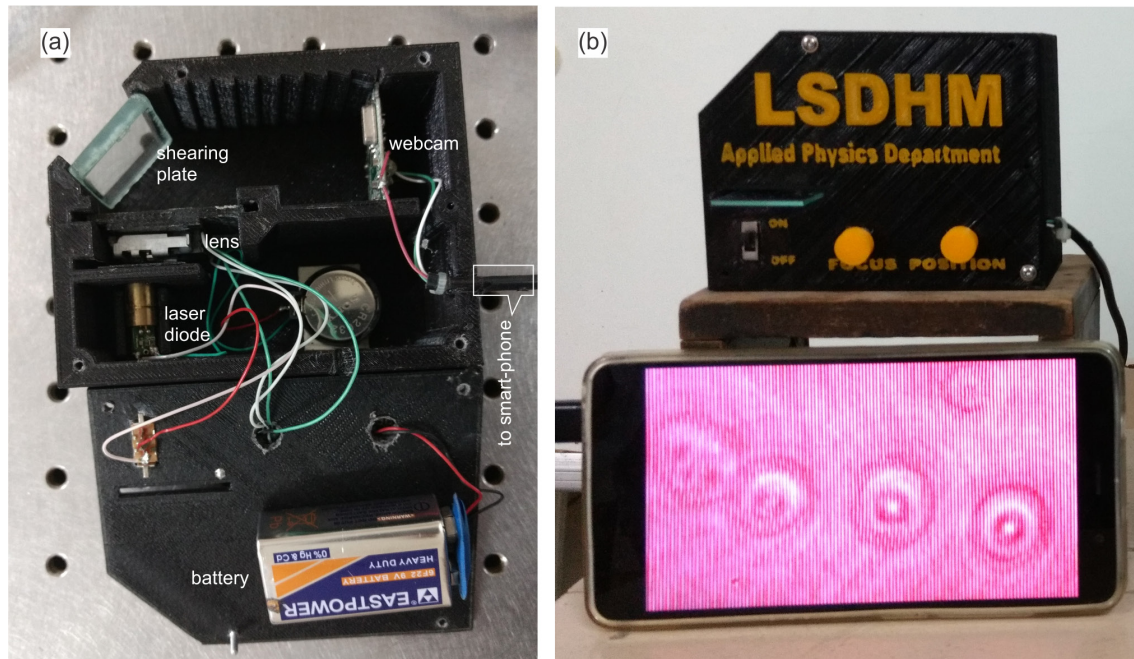


Fig. 4.12: Photograph of the 3D printed microscope. (a) Showing different components of the device. (b) Compact device attached to a smart-phone via an USB-OTG cable.

Optical components are mounted on the 3D printed support structure of the microscope. The compact LS-DHIM device has laser diode working at 635nm wavelength (output power <math><5\text{mW}</math>) as a source. The laser diode is powered by 3Volt button cell which lasted almost a day even after exhaustive use. The DVD-pickup lens having focal length 3.7mm and numerical aperture of 0.6 mounted on a voice-coil was used for magnification of the sample (Fig. 4.13). A glass plate of 5mm thickness was used for duplicating the object wavefront. The interference patterns (holograms) were recorded by USB camera sensor extracted from the web-cam having 640 x 480 resolution and  $3.2\mu\text{m}$  pixel pitch.

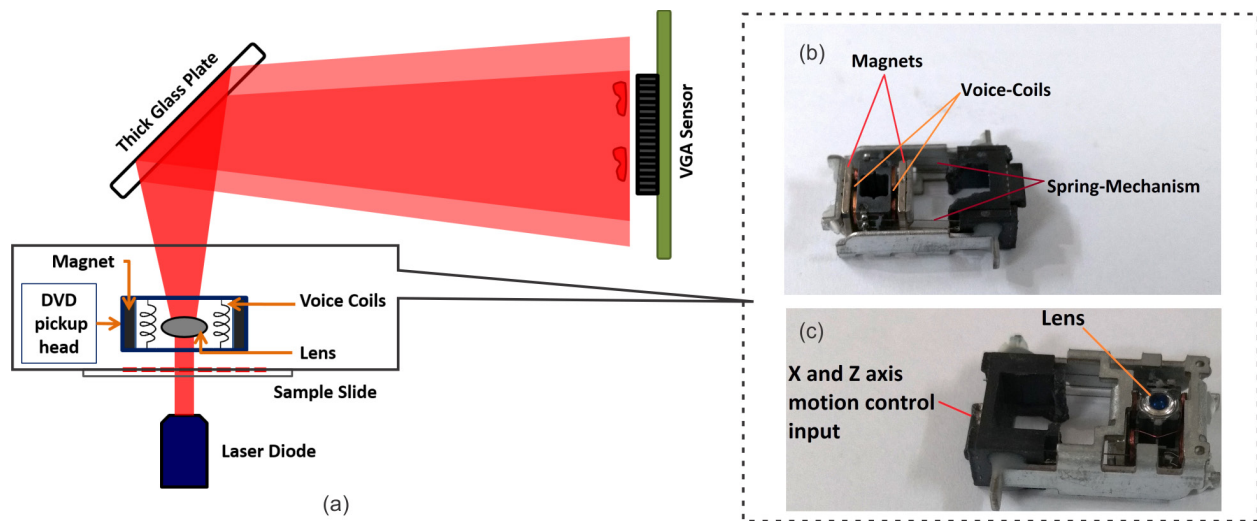


Fig. 4.13: (a) DVD pick-up unit lens mounted on voice-coil used for magnification of the sample. (b) Back and (c) Front view of the optical pick-up unit.

The focusing of the sample was achieved by applying current to the voice coil so as to move the lens mounted on it in the axial direction. Multiple filed of views were achieved also by moving the lens in the lateral direction also by applying current to the voice coil. Implementation of DVD-pickup lens significantly reduces the dimension of the device. Also, the replacement of CCD array by webcam array greatly reduces the cost of device.

Another advantage of using USB webcam sensor is that it eliminates the dependency on computers for recording holograms. Now almost all android cellphones have USB-OTG support, so that it can drive most of the peripheral devices running through USB port. The USB port of the camera can be attached to the android devices and holograms can be recorded through open-source apps available at the android playstore. The compact 3D-printed LS-DHIM along with android phone

serves as a unique field portable device (Fig. 4.12b) for analyzing physical and mechanical parameters of biological cells.

Thickness imaging capability of the portable device was tested by recording holograms of  $6\mu\text{m}$  diameter polystyrene microspheres (refractive index 1.58) immersed in microscope oil (refractive index 1.58). Portion of the hologram showing modulation of interference fringes due to the microsphere is shown in Fig. 4.14a. Phase is extracted from the numerically reconstructed hologram and the phase extracted from the reference hologram (recorded with just the immersion oil in the field of view) is subtracted from this to obtain object phase distribution shown in Fig. 4.14b.

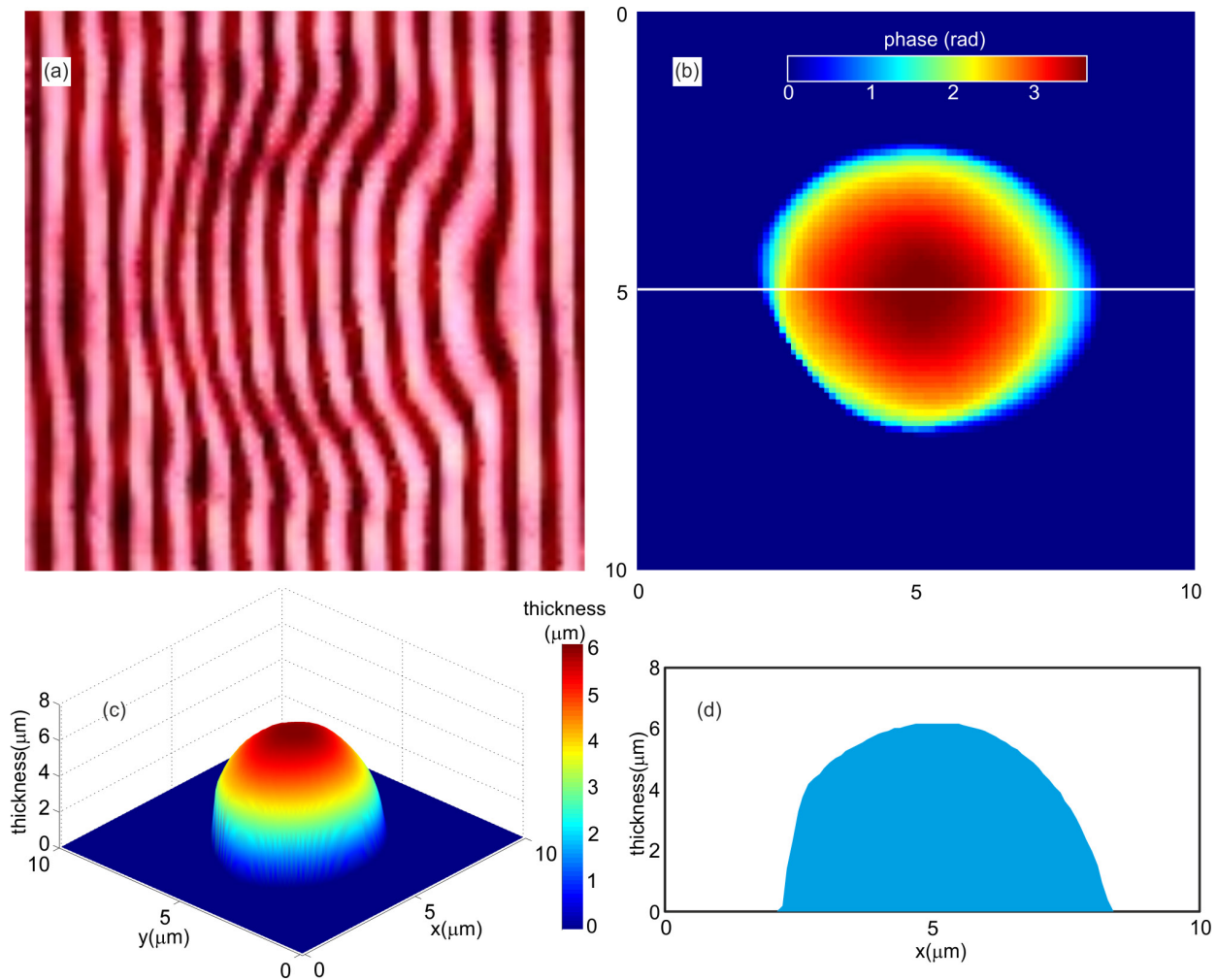


Fig. 4.14: Thickness profiling of polystyrene microspheres using portable unit. (a) Recorded hologram. (b) Numerically reconstructed phase distribution of the object. (c) Three dimensional rendering of the computed thickness distribution. (d) Cross sectional thickness profile along the direction of the white line shown in Fig. 4.14b

Spatial stability of the system determines the minimum measurable thickness. Spatial stability of the system was determined from a hologram recorded using a blank slide. Fig. 4.15a shows the thickness profile reconstructed from such a hologram. Histogram of the thickness distribution is shown in Fig. 4.15b. Standard deviation of the thickness distribution is the measure of the spatial stability of the system.

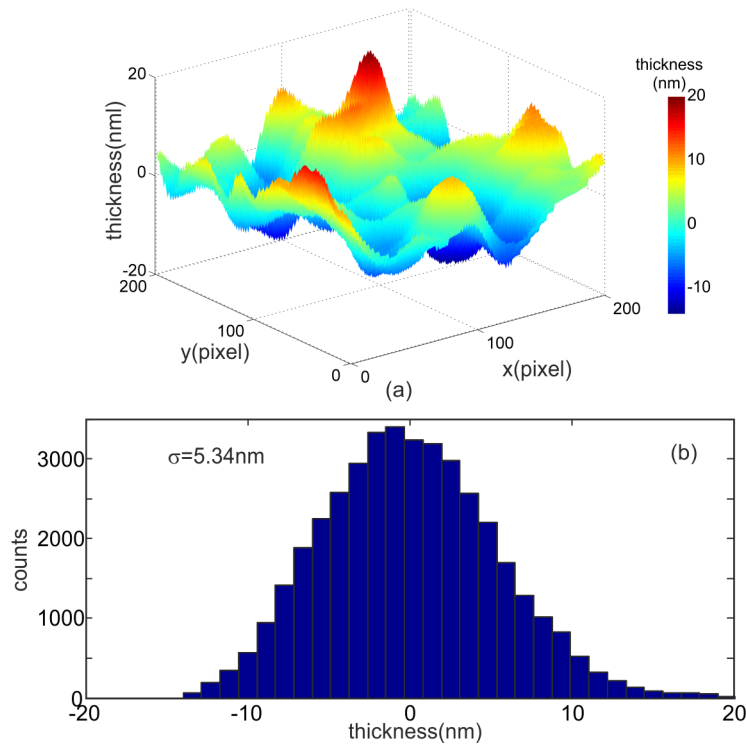


Fig. 4.15: Spatial stability of the compact system. (a) Thickness variation of the hologram recorded without the object in the field of view. (b) Histogram of the thickness distribution along with standard deviation of the distribution.

Since a webcam is used in the portable version, the expected image uniformity is low, leading to lower spatial stability. But as can be seen by comparing 4.7b with Fig. 4.15b, the spatial stability of the system employing low cost webcam array is very close to the one using a high cost CCD array. This implies that the image quality as well as the thickness measurement capability does not deteriorate much when a webcam array is used for recording of holograms.

Temporal stability of the system was determined by recording holograms of a blank slide at the rate of 25Hz (maximum allowed by the sensor) for 20s. The spatial mean of the standard deviation of time varying thickness acts as the measure of temporal stability (Fig. 4.16). In the case of compact field portable device temporal stability is above 1nm. This is because of two reasons i)

time variation in the recorded intensity by the webcam array (temporal non-uniformity of the sensor) and ii) the magnifying lens suspended on the voice coil might be changing (fluctuating) with time. But even then the device provided better temporal stability compared to two-beam devices.

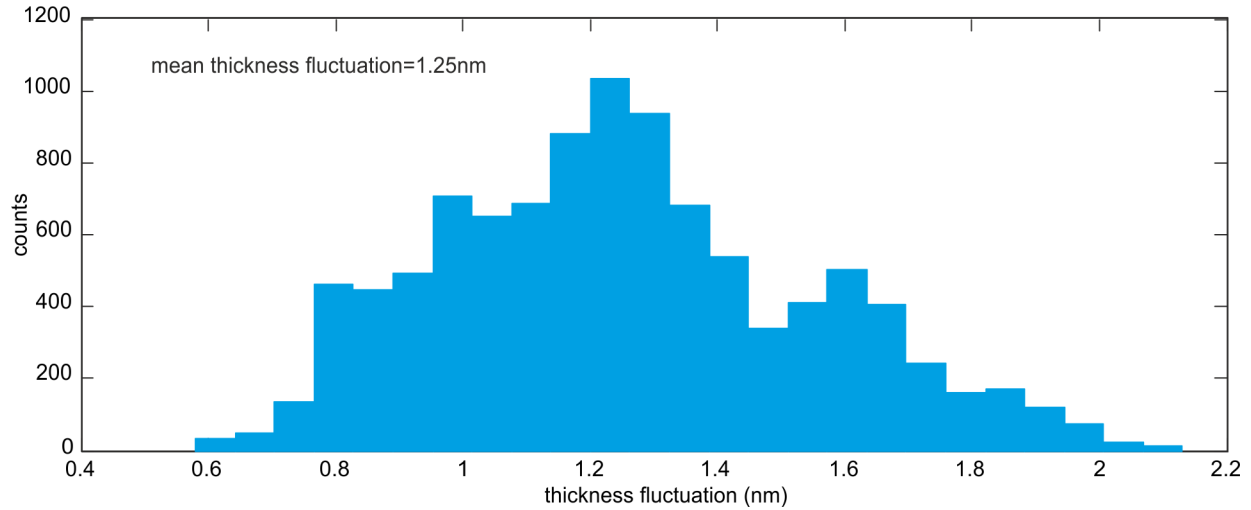


Fig. 4.16: Temporal stability of compact field portable device.

Portable device was then used to image blood cells in thin smears. Multiple field of views were achieved by applying current to the voice coil, which will move the lens laterally (only in one direction). The device can provide 20 field of views amounting to an area of approximately  $800\mu\text{m} \times 40\mu\text{m}$ . Fig 4.17 shows the multiple holograms (field of views) obtained by laterally translating the imaging lens

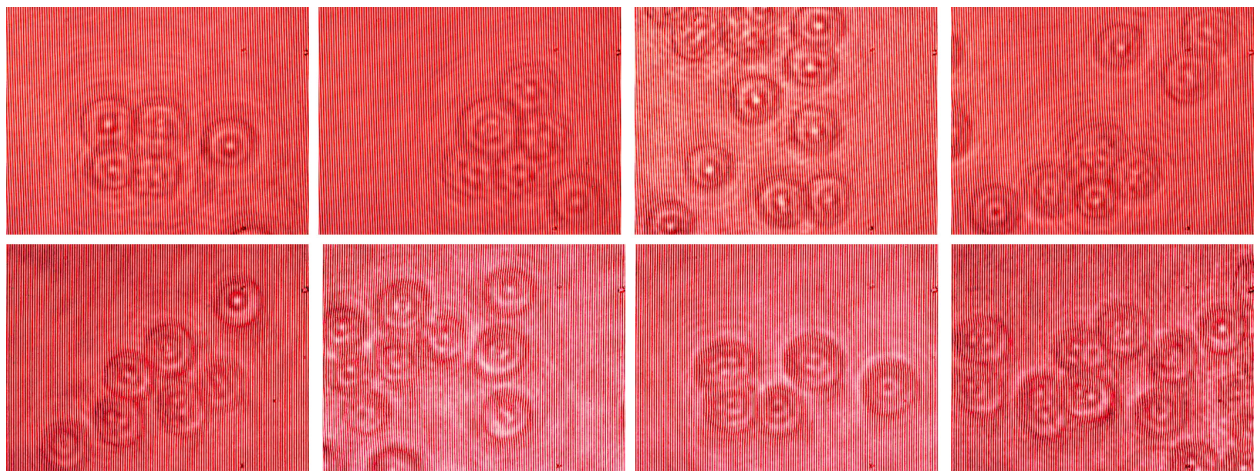


Fig. 4.17: Holograms of red blood cells recorded by translating the magnifying lens laterally.

A single reference hologram was used to extract the object phase information from all the object holograms. Fig. 4.18 shows the quantitative phase image of blood cells obtained after stitching together multiple field of views.

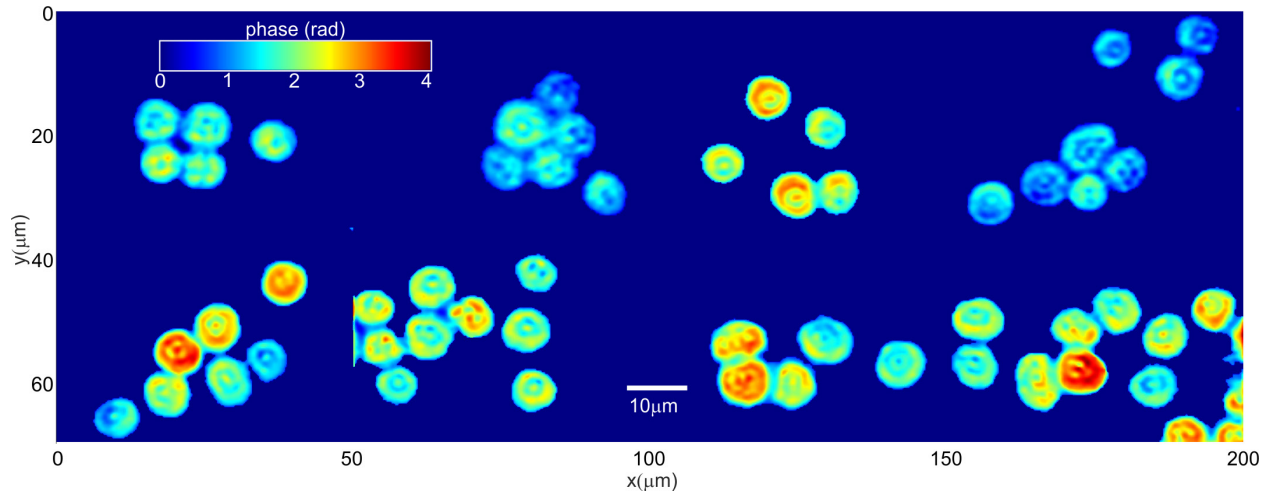


Fig. 4.18: Quantitative phase images of blood cells obtained by stitching together multiple field of views  
Phase distribution when plugged into Eq. (3.9) provides the optical thickness profile of the cells in the field of view (Fig. 4.19).

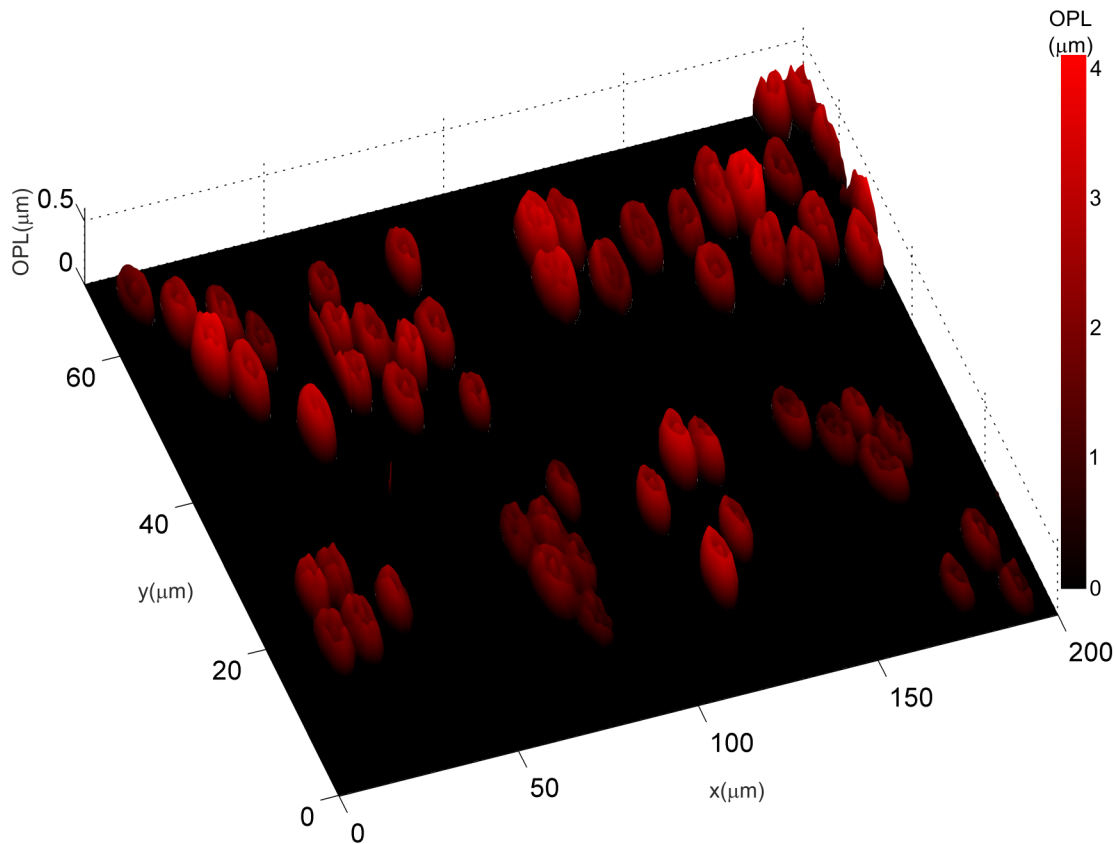


Fig. 4.19: Blood cell thickness distribution obtained using phase map in Fig. 4.18

Cell thickness distribution can be used to obtain several physical and mechanical parameters of the blood cells described in Section 3.5. These parameters will depend upon the state of health of the cells and could be used to classify them. The compact device can be attached to a cell phone via a USB-OTG cable to record holograms as well as to transmit (holograms) and receive (cell parameters) obtained from processed holograms. The numerical reconstruction of holograms as well as data extraction can be done in an off-site server (Fig. 4.20). The database contained in the server can be used to identify, compare and classify cells, which may lead to disease identification without the need of a trained technician.

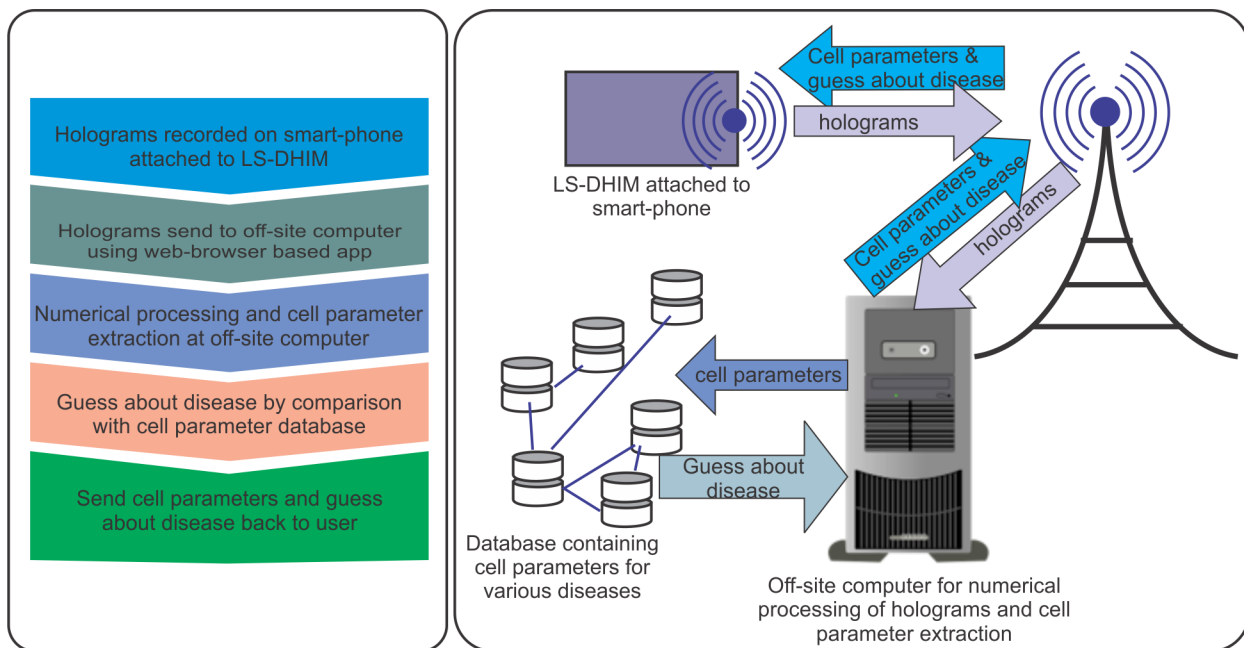
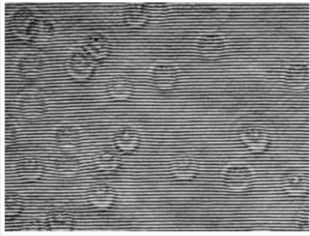
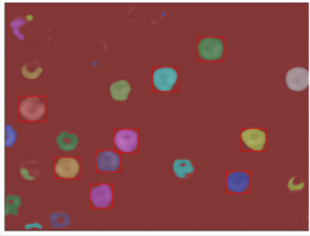
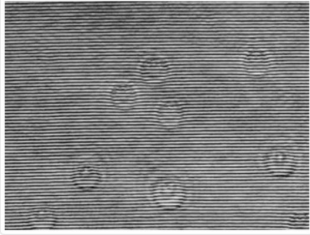


Fig. 4.20: Point-of-care application of the portable LS-DHIM

An In-house developed code in Python was placed in the off-site computer for numerical processing of the holograms. The holograms were transmitted to this computer via mobile internet using an in-house built, browser-based application (Fig. 4.21a). The holograms received by the server were numerically processed to obtain the phase maps. The cell thickness information is computed from the phase maps and physical and mechanical cell parameters were extracted. The phase maps and along with the extracted cell parameters are transmitted to the user (Fig. 4.21b) along with an educated guess about the disease affecting the sample. User (who can be a medical practitioner) can take a decision towards the next step required using the information supplied by the microscope.

## List of images

Shows list of all images

ID	Analyze	Name	Link	Image	Processed Image	
5	Analyze	7	Parameters			<a href="#">Open</a>
6	Analyze	16	Parameters			<a href="#">Open</a>

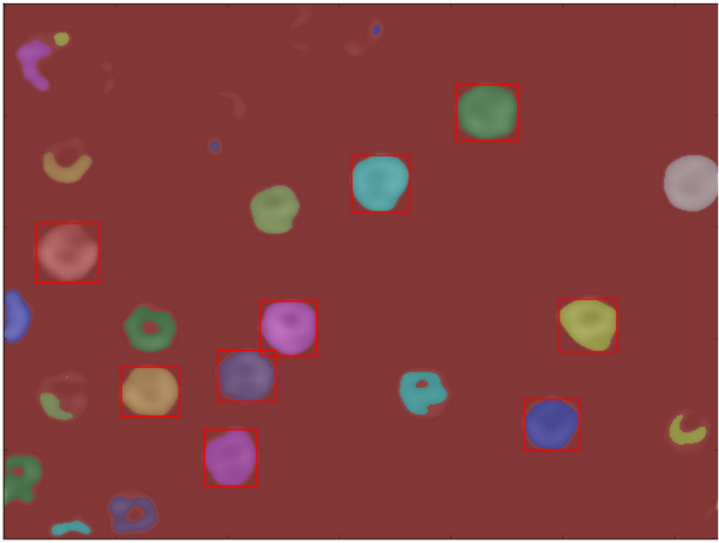
(a)

List of images

Shows list of all images

ID	Analyze
5	Analyze
6	Analyze

Processed Image



[Open](#)

[Open](#)

```
volume:1.44831782485568E-17
mean_thick:3.42098702553121E-07
max_thick:0.4773466701
std_thick:0.0856978761
CV_thick:0.2505062879
PA:4.2336256E-11
PA/vol:2923132.98044362
Dia:7.3419476513546E-06
CSA:4.37147282627193E-11
SA:8.60509842627193E-11
Sph:0.3339162333
```

(b)

Fig. 4.21: (a) Sending data (hologram) to the off-site computer. The computer processes the holograms and extracts the cell parameters. (b) Cell parameters and the phase maps are send back to the user.

#### 4.5 Transforming bright field microscope to digital holographic microscope

One of the challenging problems is to convert an existing bright field microscope into a quantitative phase microscope with minimum alterations. Some the research groups around the world are using quantitative phase imaging modules that can be retrofitted to a conventional bright field microscope to obtain cell thickness profiles [69]. Lateral shearing DHIM provides an opportunity to convert clinical microscopes into 3D microscopes with minimum alterations. A compact lateral shearing quantitative phase imaging module was designed that could be attached to a standard bright field microscope, converting it into a quantitative phase imaging one (Fig. 4.22). A 20 $\times$  microscope objective with numerical aperture of 0.4 was used for magnification of the sample.

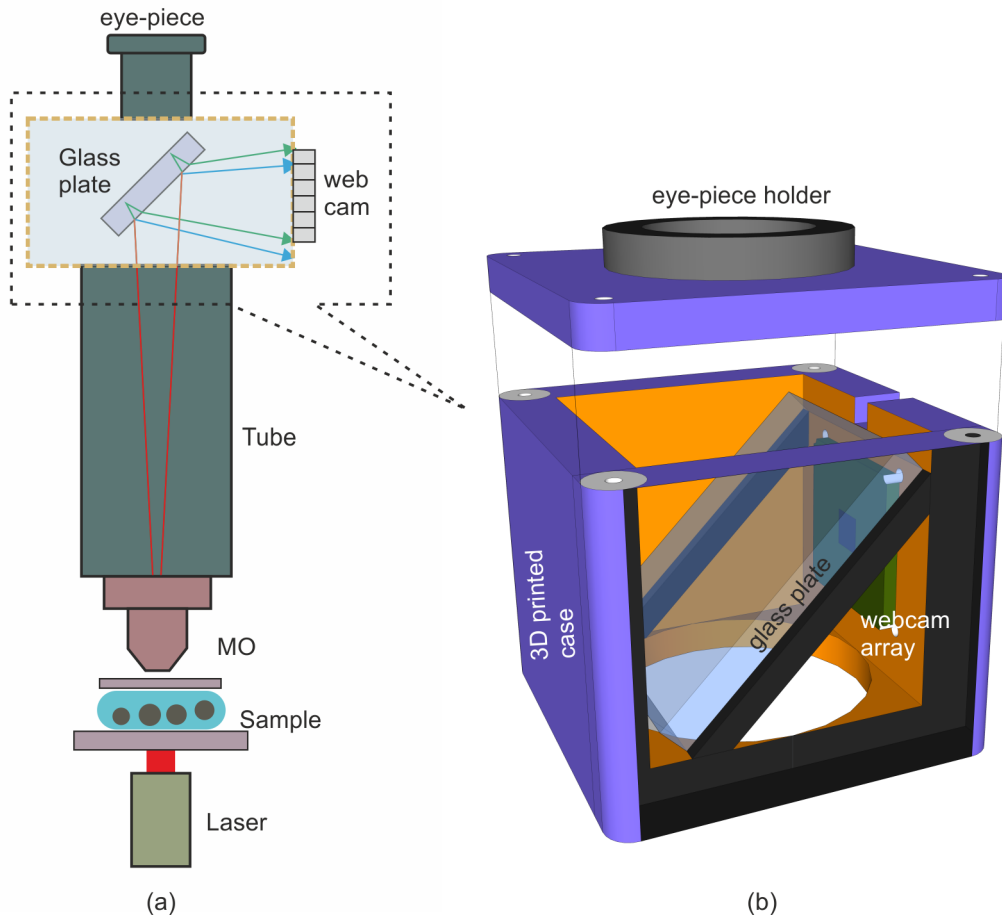


Fig. 4.22: Converting bright field microscope to quantitative phase imaging microscope. (a) Optical alignment and laser beam ray path. (b) 3D printed quantitative phase imaging module.

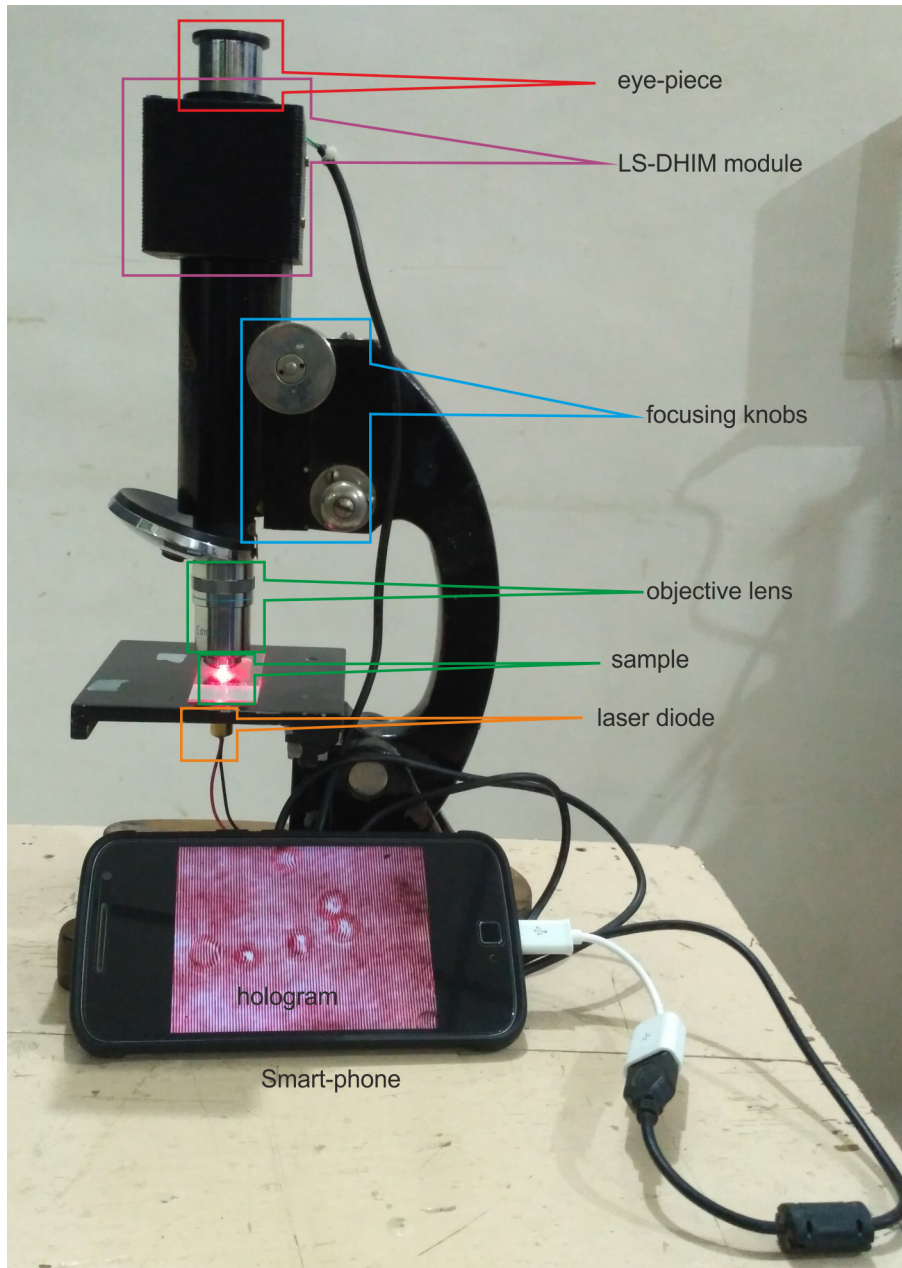


Fig. 4.23: Microscope fitted with quantitative phase imaging unit.

Bright field microscopes were retrofitted with the 3D printed quantitative phase imaging module as shown in Fig. 4.22a. On one of the apertures below the sample holder a 635nm laser diode was fixed. For conventional bright field images, the laser diode module was rotated out from below the sample and broadband source was used for illumination. The quantitative phase imaging module (Fig. 4.22b) was introduced at the end of the microscope tube. Light passing through the sample

encounters a glass plate of thickness 5mm. Most of the light falling on the glass plate is transmitted. This is ideal for bright field images observed through the eye-piece, which is mounted on the top of the quantitative phase imaging unit. Eye-piece could be removed, and an imaging sensor could be used instead leading to acquisition of amplitude contrast images. Two laterally sheared versions of the object wavefront will be reflected from the glass plate. They interfere at the sensor plane forming holograms. A VGA (640×480 pixel) color webcam array was used to record the holograms. The webcam was connected to a smart-phone through a USB-OTG cable. Fig. 4.23 shows the photograph of a microscope fitted with the quantitative phase imaging module. Smart-phone acted as the hologram recording device. The recorded hologram movies were then processed to compute the sample thickness profile.

Fig. 4.24a shows the recorded holograms (object holograms) of 10 $\mu$ m diameter polystyrene microspheres sandwiched between a microscope slide and a cover glass and immersed in microscope oil. As in the previous cases, a reference hologram of the medium (Fig. 4.24b) surrounding the microspheres were also recorded for phase subtraction.

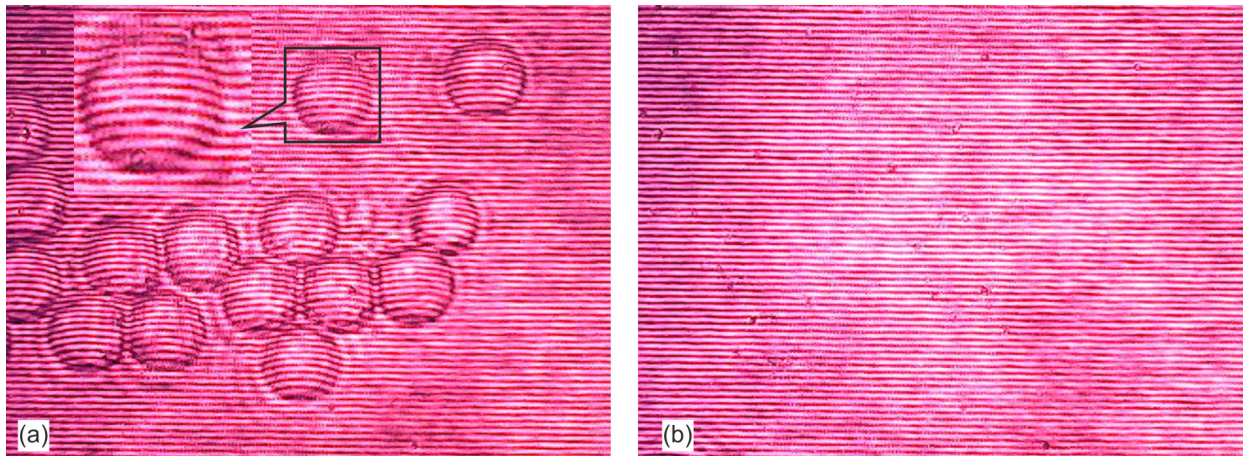


Fig. 4.24: Holograms recorded using the bright field microscope fitted with the 3D imaging module. (a) Object hologram. (b) Reference hologram

Object and reference holograms were reconstructed separately and their phases were extracted separately. Subtraction of the reference phase from the object phase nullifies most of the phase due to aberrations and brings out the object phase distribution, which is shown in Fig. 4.25a. The reconstructed phase distribution was used along with the refractive index values of the microspheres (1.58) and that of the microscope immersion oil (1.52) in Eq. (3.9) to compute the thickness profile of the microsphere, which is shown in Fig. 4.25b. The average of the measured

diameter of the microspheres was  $9.42\mu\text{m}\pm 1.34\mu\text{m}$ , which is very close to the manufacturer specified value of  $10.0\mu\text{m}\pm 1.0\mu\text{m}$ , which basically shows the thickness profiling capacity of the microscope

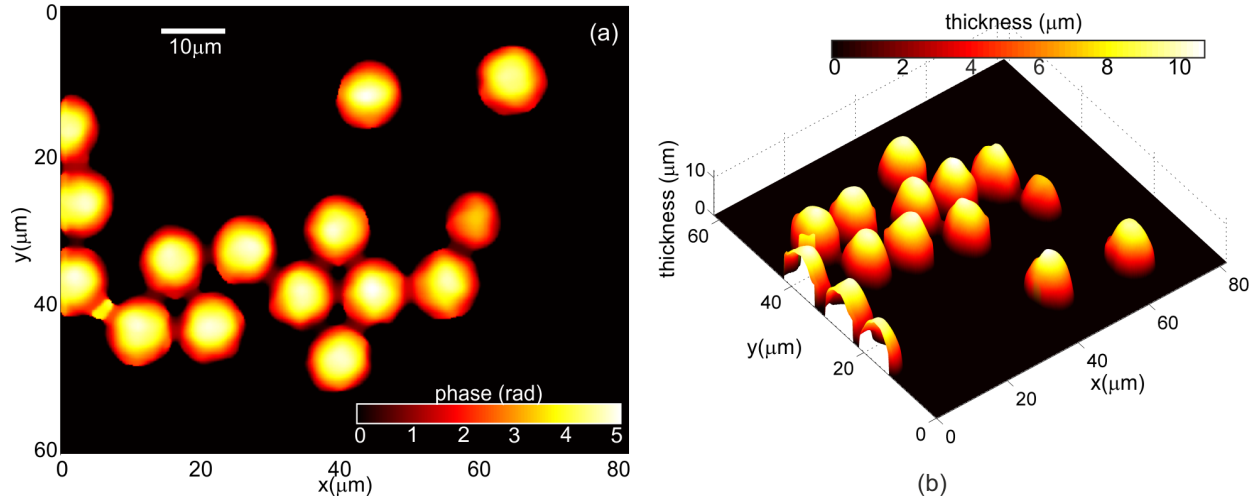


Fig. 4.25: Quantitative phase imaging using bright field microscope fitted with the 3D imaging unit. (a) Phase distribution of  $10\mu\text{m}$  diameter polystyrene microspheres. (b) Three dimension rendering of the computed thickness distribution.

The developed microscope was then used for thickness profiling of red blood cells. Recorded hologram in the case of red blood cells is shown in Fig. 4.26a. The optical thickness distribution of red blood cells obtained after phase subtraction is shown Fig. 4.26b.

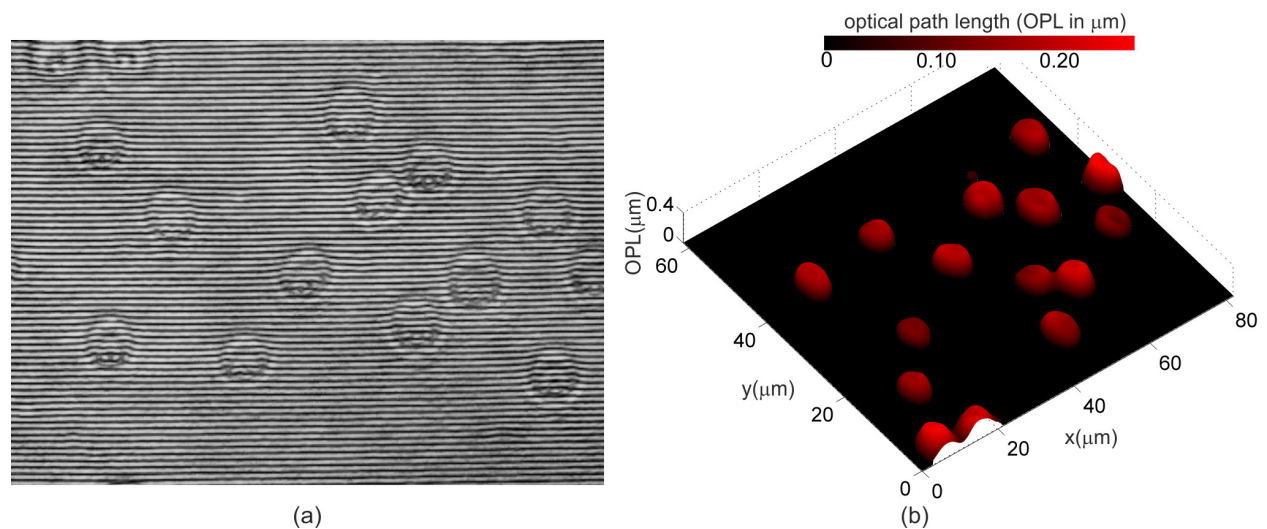


Fig. 4.26: Quantitative phase imaging of red blood cells using bright field microscope fitted with the 3D imaging unit. (a) Recorded hologram. (b) Three dimension rendering of the computed thickness distribution.

## 4.6 Conclusions

Two-beam DHIM, techniques like MZ-DHIM many optical elements for beam splitting, beam steering and beam recombination, making such setups bulky and not suitable for on-field applications. Compared to such setups, lateral shearing, self-referencing common path technique described in this chapter provides a compact and stable structure utilizing very few optical elements. It makes it highly temporally stable, with sub-nanometer stabilities over long periods of time [17, 93]. Since the technique requires very few optical elements, hand-held versions of the microscope can be easily constructed by 3D printing the microscope structure. A low-cost version of the device was constructed using DVD pick-up lens mounted on voice coil for magnification of the sample as well as generation of multiple field of views and a webcam sensor for recording of the holograms. One of the interesting findings during this work was that a webcam array provided spatial and temporal stabilities comparable to that of CCD arrays and the quality of the reconstructed quantitative phase images also were comparable with those using CCD array. Software were developed in-house for sending the hologram from the user smart-phone to off-site computer, where the numerical processing and parameter extractions from recorded holograms takes place. Python based code was deployed on the computer for numerical processing of the holograms. The extracted parameters were send back to the user. The main drawback of the LS-DHIM is that it can handle sparse object distributions only, since one requires object free wavefront to act as the reference. But this drawback is compensated by its compact nature, easy of fabrication and field portability. The field portable instrument has the potential to be very useful in point-of-care application.